

Absorption, transmission, and scattering of expanded polystyrene at millimeter-wave and terahertz frequencies[†]

Charles R. Dietlein^{a,b,‡}, Jon E. Bjarnason^b, Erich N. Grossman^b, and Zoya Popović^a

^aDepartment of Electrical and Computer Engineering, 425 UCB, University of Colorado at Boulder, Boulder, CO, 80309

^bOptoelectronics Division, National Institute of Standards and Technology, 325 Broadway, MC 815.04, Boulder, CO, 80305

ABSTRACT

Conventional material measurements of transmission and reflection in the millimeter-wave and terahertz frequency range do not differentiate between scattering and absorption, grouping effects from both mechanisms together into “loss”. Accurate knowledge of the balance between scattering and absorption is critical in applications such as radiometric scene modeling for concealed object detection, where evaluation of object detectability depends strongly on the amount of scattering due to concealers such as clothing. We describe an experimental setup for the measurement of spatial bidirectional reflectance distribution function (BRDF). Previous measurements have shown extremely low-level grating lobes from periodic clothing materials such as corduroy, around 30 dB below the transmitted beam. To adequately address this issue of high dynamic range, we utilize a cryogenic antenna-coupled microbolometer for detection. We present data on several types of expanded polystyrene, a common structural material for systems and experiments in this frequency range. In these measurements of BRDF, transmission agrees with previous measurements, and the balance between low and high angle scattering, specular reflectance, and absorption is examined.

Keywords: absorption, BRDF, expanded polystyrene, material measurement, millimeter-wave, scattering, terahertz

1. INTRODUCTION

Conventional measurements of millimeter-wave and terahertz material loss simply measure the decrease in power coupled from source to detector when a sample is introduced. They therefore do not distinguish between absorption and scattering; effects such as grating lobes due to periodic structure are neglected, and beam broadening in reflectivity measurements due to diffuse reflectance from, e.g., surface roughness, is not measured.

The distinction between scattering and true absorption is an issue in both active and passive millimeter-wave/terahertz imaging. Figure 1 pictorially demonstrates the extreme cases of concealers’ material properties being strongly scattering, reflective, and absorbing, for both imaging modalities. In the active modality, thermal emission from the body, concealer, and concealed object are assumed negligible; the transmitted radiation is orders of magnitude greater than the blackbody radiation, and the detector does not have the dynamic range required to receive both thermal emission and reflected incident radiation simultaneously. In the passive modality, thermal emission is assumed dominant; a sensitive detector (cryogenic or heterodyne) is typically used. Previous work has measured transmission through clothing samples in the millimeter-wave and infrared regimes¹, but did not specifically consider scattering. The precise distinction between scattering and absorption plays an important role in radiometric scene simulation^{2,3}, as well as the scattering/reflectance balance of building materials. A reflectometer has been built to measure broadening of specularly-reflected radiation for the latter purpose⁴, and is essentially a predecessor to the system described in this paper.

Besides imaging applications, engineering of systems in this frequency range often require extremely low-loss materials. One example of a system requiring a low-loss structural material is the Aqueous Blackbody Calibration source⁵. The ABC source is a water-based broadband blackbody emitter for the millimeter-wave/terahertz frequency regime. Its upper cutoff frequency is currently determined by the balance between scattering and absorption in the

[†]Contribution of the U.S. government. Not subject to copyright.

[‡]e-mail: dietlein@boulder.nist.gov, phone: +1 303 497 4843

expanded polystyrene (EPS) container that holds the water in its specific geometry. The effect is as follows: instead of the physical temperature of the water being equal to the radiometric temperature (as desired), the latter is decreased due to a finite amount of loss in the EPS. If all measured loss is considered to be absorption and the reflected radiation from the EPS is negligible, then the radiometric temperature of a bath of water behind an EPS wall is reduced by an amount equal to the fractional absorption multiplied by the mean of the ambient and water temperatures. On the other hand, if the loss is not absorption, but rather scattering, the radiometric temperature will be much closer to that of the physical water temperature. Previous measurements of polystyrene foam focused on determination of the dielectric constant, but were not sensitive to scattering, though scattering was suggested as a probable loss mechanism⁶. Scattering in the case of the ABC source EPS is looked at as a favorable alternative to absorption, and indeed the expected extinction mechanism.

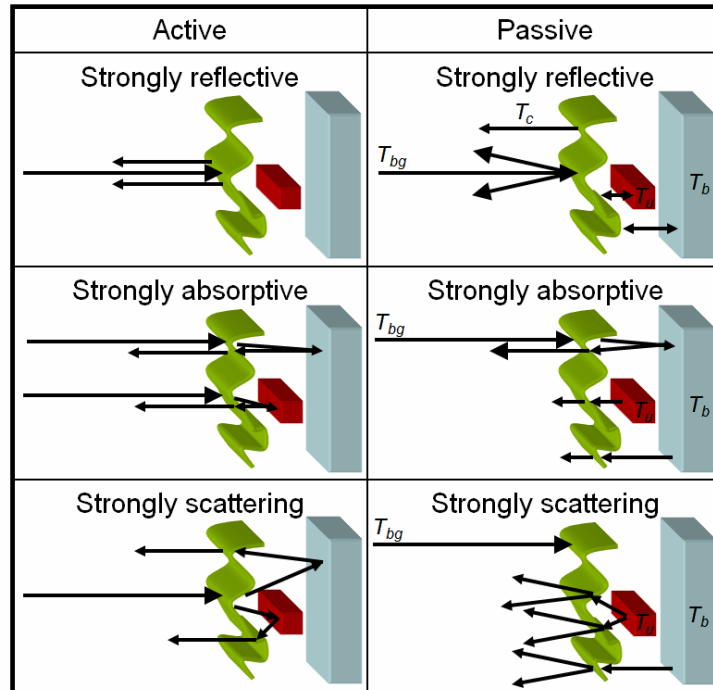


Fig. 1. A graphical depiction of active and passive imaging modalities with three extreme cases of concealer (left-most “squiggle” surface): strongly reflective, strongly absorptive, and strongly scattering. In the active case (left), the only source of incident radiation considered is from the imaging system. In the passive case (right), the concealer (c), background (bg), body (b), and unknown object (u) each have physical temperatures and emissivities that contribute to the final radiometric image.

2. EXPERIMENTAL SETUP

2.1 Hardware

A superconducting ($T = 4.2$ K) antenna-coupled microbolometer⁷ is located in a liquid helium-cooled cryostat on a platform approximately 0.5 m above an optics table. The self-complementary spiral antenna has a design frequency range of 0.1 THz to 1.8 THz and is circularly polarized. The microbolometer is voltage biased and operated with room-temperature electronics⁸ providing negative electrothermal feedback⁹. Cooled filters at 77 K and 4 K prevent infrared radiation from saturating the detector, and a 4 mm diameter hemispherical substrate lens is located above the antenna to prevent substrate modes, reduce the silicon-vacuum interface reflection, and increase antenna directivity¹⁰. A three-way periscope is affixed to an arm mounted on a rotation stage, with the center of rotation collinear with the vertical axis of the sample under test. The arm length is 33 cm from the rotation axis to the center of the first periscope mirror, and the total length of the periscope path from the sample rotation axis to the detector is 122.5 cm. Due to physical limitations (the walls of anechoic material and the cryostat platform legs) the arm is able to revolve from approximately $\theta_A = -20^\circ$ to $\theta_A = 160^\circ$, where $\theta_A = 0^\circ$ is the intended location of the transmitted source beam. In reflectance measurements, arm angle

θ_A is related to beam incidence angle by $\theta_i = (180 - \theta_A)/2$. The source is a backward wave oscillator (BWO) operated between 800 GHz and 900 GHz and linearly polarized. The electric field is oriented 8° from parallel to the optics table, which is also the plane of incidence in the reflectance measurements described in Section 3. This angle was separately measured by rotating a wire grid polarizer through the beam. Because the polarization is neither purely parallel nor perpendicular to the plane of incidence, a vector superposition of the Fresnel formulae for reflectance is required, and as discussed in Section 3.2, the extraction of material parameters can be quite sensitive to the electric field orientation. The BWO beam is baffled by a circular aperture 19.1 mm in diameter at the entrance of the scattering measurement experiment, 17.8 cm from the sample. The power vs. angle measurement with no sample present is defined primarily by the baffling; measured beamwidth and sidelobe spacing agree with the predicted Airy pattern from a circular aperture. Walls of radar-absorbing material are placed between the setup and the BWO source to block stray radiation. The incident beam is mechanically chopped at the circular aperture, and a lock-in amplifier is used to measure the detected signal through the previously-mentioned electronics⁸. Lock-in amplifier readings (R, in Volts) are proportional to power.

To validate the setup, a small ribbon cable with wire pitch $p = 0.5$ mm was placed in the sample position, normal to the incident beam. The first grating lobe peak should appear at $\arcsin(\lambda/p) = 43.6^\circ$ for $f = 877$ GHz, and it was observed at 43.8° , 14.7 dB down from the peak power of the transmitted beam with no sample present (Figure 3). The transmitted beam maximum is at $\theta_A = 0.25^\circ$, so the grating lobe is just 0.05° from the expected location. The arm is operated by a stepper motor with absolute positioning accuracy of 0.01° .

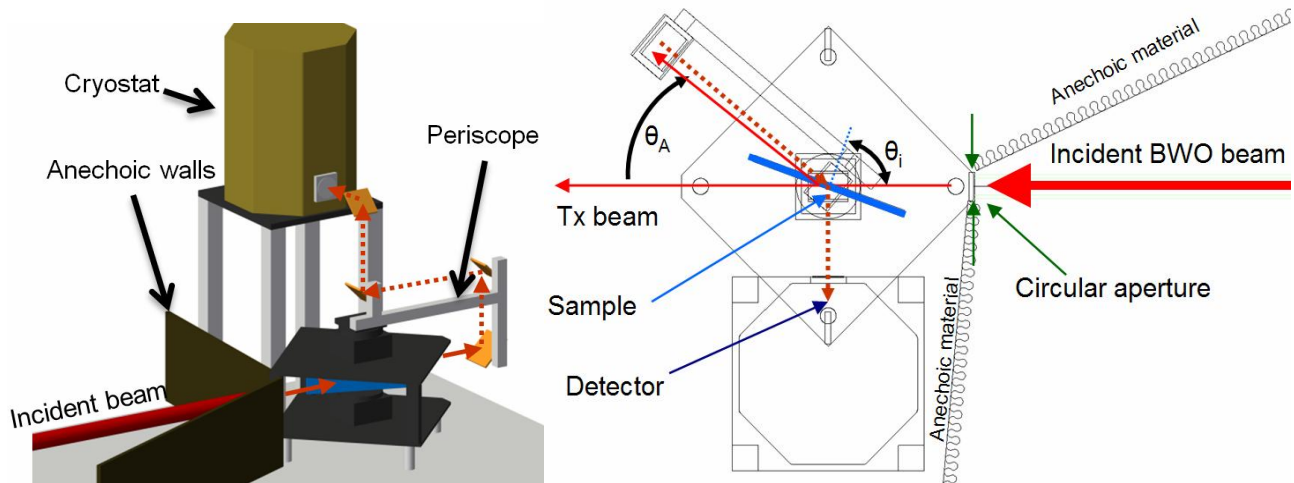


Fig. 2. Two views of the experimental setup: (left) A rendering showing the geometry of the incident beam, baffling, rotation-arm-mounted periscope, and cryostat. (right) Top view of the same setup. The backward-wave oscillator (BWO) beam enters the measurement setup from the right side of this view. A sample under test is drawn at an angle of approximately $\theta_i = 70^\circ$. Arm angle is referenced from the Tx beam at $\theta_A = 0^\circ$. For clarity, the beam paths from the sample to the bottom periscope mirror and from the top periscope mirror to the bending mirror at the arm axis of rotation are offset. In both the left and right views, the dotted line indicates a beam path that is out of the plane of the sample and BWO beam.

2.2 Procedure

Two experiments were performed to gather information about the EPS samples. First, transmission measurements for samples at normal and $\theta_i \sim 45^\circ$ incidence angles were completed. In this measurement, the periscope arm was rotated $\theta_A = \pm 20^\circ$ to detect any steering of the transmitted beam and/or beam broadening, deformation, or grating lobes. Second, specular reflectance from EPS samples was examined. Due to the large dynamic range between the transmitted beam and the specular reflected signal, the beam was attenuated by approximately 20 dB so that the transmitted beam and specular reflection could be obtained with the same lock-in amplifier settings in a single arm sweep, for an accurate comparison of transmitted and reflected power levels. For some low-density samples, the attenuation had to be removed to accurately measure the specularly reflected beam shape, due to the extremely low level of reflected power.

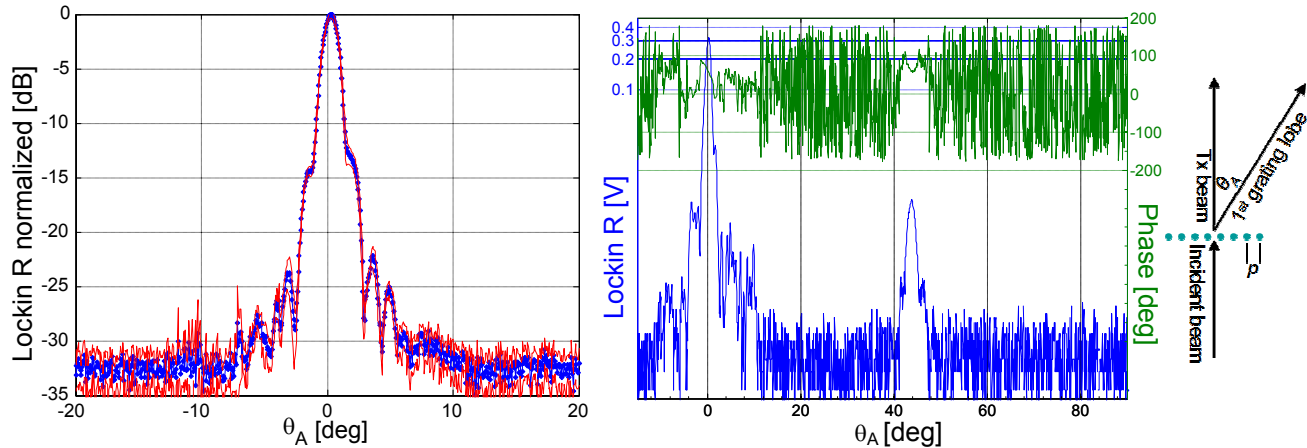


Fig. 3. (left) Mean of ten scans of the beam, with no sample installed, normalized to the maximum and shown in dB. The outline indicates ± 1 standard deviation from the mean. The noise floor is typically 33 dB below the main beam maximum with a lock-in amplifier time constant of 100 ms. The full-width half-maximum (FWHM) beamwidth is approximately 1.3° , with peak beam power stability ± 0.05 dB. (right) Measurement of the first grating lobe from a ribbon cable with wire spacing $p = 0.5$ mm at a BWO frequency of 877 GHz (representative schematic at far right).

2.3 EPS material parameters

Commercial EPS has two parameters: pre-expansion bead diameter d , and final target EPS density. The three commonly available pre-expansion bead diameters are: $d < 0.5$ mm; $0.5 \text{ mm} < d < 0.7$ mm; and $0.7 \text{ mm} < d < 1.0$ mm. The diameter distributions within each bead size category are approximately Gaussian due to the nature of the sorting process¹¹. More specific bead diameters can be attained with additional sorting meshes, if desired. Final EPS densities between 15 g/L and 130 g/L are easily manufactured. This density is a combination of the raw polystyrene density and the density of air and blowing agent that remains in the EPS once the expansion process is complete. For comparison, most standard hot beverage containers are made from the smallest bead size, with a density of approximately 90 g/L. We measured four different variations of EPS: $d < 0.5$ mm, 35 g/L; $d < 0.5$ mm, 120 g/L; $0.5 \text{ mm} < d < 0.7$ mm, 35 g/L; and $0.5 \text{ mm} < d < 0.7$ mm, 54 g/L. The samples were provided in sheet format and were each 1 cm thick. Bulk polystyrene has a refractive index of $n = 1.6$ between 200 GHz and 1 THz¹² and a density of 1050 g/L, so based on EPS density, the “effective” refractive indices of our samples should be 1.02 (35 g/L), 1.03 (54 g/L), and 1.07 (120 g/L). In other work, measurements of three samples of polystyrene foam with densities between 30 g/L and 40 g/L produced refractive indices between 1.017 and 1.022 in the 200 GHz – 4 THz frequency range⁶.

3. RESULTS

3.1 Peak transmitted beam attenuation

The peak transmitted beam power attenuations are given in Table 1. In previous measurements with a Fourier-transform infrared spectrometer (FTIR), EPS with $0.5 \text{ mm} < d < 0.7$ mm, and density of 54 g/L had a transmittance T of -0.7 dB, and for the 35 g/L sample T was -0.4 dB, all at the same frequency as in the current experiment, 877 GHz. A $d < 0.5$ mm, 35 g/L sample had a T of -0.4 dB as well, and for a 96 g/L sample of the same bead size (not available for this paper), T was measured to be approximately -3.5 dB. The FTIR data follow the same trend as the newly-acquired data. Based on the results here, with transmittance measured at two separate angles, as well as the effects found in Section 3.3, it is plausible that the differences in actual measured transmittance values could be due to slight misalignment of the sample in the FTIR. Additionally, we note that the SNR in the FTIR is orders of magnitude lower than the SNR utilizing the BWO and cryogenic microbolometer, and the actual FTIR data below 1 THz is the result of a fit due to low SNR. Thus, the trend found with the FTIR matches the trend here, in terms of bead diameter and density, but the exact attenuation values found in both experiments are subject to the specific sample, exact orientation, and other environmental variables. Excess loss in EPS with density above 35 g/L can be attributed to the trapping of water inside the polystyrene bead matrix during the expansion process, when high temperatures and steam are utilized. In this process, the EPS is cooled while steam and blowing agent still reside within the cell matrix, trapping an unknown

amount of particulate water between the inner-most cells of the EPS sheet. The blowing agent used in the process for this EPS is pentane, C₅H₁₂.

The expected theoretical result for dielectric slab transmittance is¹³:

$$T_{slab} = |t_{slab}|^2 = \frac{(I-R)^2 + 4R \sin^2(\psi)}{R^2 e^{-\alpha h} + e^{\alpha h} - 2R \cos(\zeta + 2\psi)} \quad (1)$$

where

$$\psi = \tan^{-1}\left(\frac{2k}{n^2 + k^2}\right), \quad \zeta = \frac{4\pi n h}{\lambda}, \quad \alpha = \frac{4\pi k}{\lambda}, \quad R = \left|\frac{1-\tilde{n}}{1+\tilde{n}}\right|^2, \quad \tilde{n} = n + ik,$$

and h is the slab thickness. Equation (1) is the exact expression that applies only to a monochromatic field and perfectly smooth dielectric slab walls. In reality, these conditions are closely approximated but never achieved, which leads to an expression in which coherent interference does not appear. In our situation, the EPS surface roughness of greater than the Rayleigh criterion, $\lambda/(8\cos\theta_i)$, blurs the coherent effects; additionally, the interior of the EPS slab is inhomogeneous compared to an ideal dielectric slab. Thus, the transmittance approximation neglecting coherence, in the limit of transparency ($R^2 e^{-2\alpha h} \ll I$) is:

$$T_{slab} = (1-R)^2 e^{(-\alpha h)}. \quad (2)$$

Equation (2) can be used as a first-order approximation to the transmission and reflection, by using the material properties for bulk polystyrene and calculating an “effective” complex refractive index based on EPS density and loss coefficient¹². This is the limiting case in which scattering is not considered, and even for the densest EPS sample, only 1.11 dB of transmission loss is calculated at normal incidence for density-adjusted $k = 6 \times 10^{-4}$ (from bulk polystyrene measurements of k in reference 9) and $n = 1.07$.

Table 1. Peak measured transmitted beam attenuation at $f = 877$ GHz. The top entry in each cell is attenuation for normal incidence, and the bottom entry is for 45° incidence. The asterisk indicates a measurement where the actual loss was less than the noise or stability of the measurement.

		Density		
		35 g/L	54 g/L	120 g/L
Bead size	$d < 0.5$ mm	0.24 dB	n/a	2.1 dB
		0.64 dB		5.6 dB
	$0.5 \text{ mm} < d < 0.7$ mm	0*	0.8 dB	n/a
		0.3 dB	0.7 dB	

3.2 Specular reflectance

In measurements of specular reflectance, both the front and back surfaces of the EPS sample were distinguished due to the finite thickness of the samples. An example of raw data is shown in Figure 4. As expected, the received power reflected from the front surface of the EPS is slightly greater than that received from the back surface reflection. The refractive index of the sample can be calculated based on the Fresnel equations and measured reflectance values (R),

$$\sqrt{R_{\parallel}} = r_{\parallel} = \frac{\cos \theta_t - n \cos \theta_i}{\cos \theta_t + n \cos \theta_i} \quad (3)$$

and

$$\sqrt{R_{\perp}} = r_{\perp} = \frac{\cos \theta_t - n \cos \theta_i}{\cos \theta_t + n \cos \theta_i}. \quad (4)$$

The reflectance results are compiled in Table 2. It is important to be aware that the accuracy of the polarization of the incident beam and θ_i are key in extracting n from measured reflectance, in the limit of n approaching 1. The angle θ_i

is known extremely accurately due to measurement of the angle between the transmitted and specular reflected beams, from the stepper motor controlling the arm. The polarization of the incident field was measured and found to be at 8° from parallel to the plane of incidence, $\pm 2^\circ$. This corresponds to a worst-case uncertainty in n of ± 0.02 . The resulting extracted refractive indices from measured data in Table 2 are as follows: for the 35 g/L, $0.5 \text{ mm} < d < 0.7 \text{ mm}$ sample, $n = 1.035$, similar to the results with the 35 g/L polystyrene foam in reference 3. For the 54 g/L sample, $n = 1.067$, and for the 120 g/L sample with the smallest beads, $n = 1.15$. The last value, $n = 1.15$, is higher than expected, but is explained; due to the nature of the molding process, there exists a thin layer of expanded polystyrene that has a refractive index closer to the bulk value ($n = 1.6$) than the average that is due simply to density. It is known that the refractive index of expanded polystyrene beads varies as a function of bead radius¹⁴, with 1.6 being the maximum value, naturally found at the outermost “shell” of the bead. In the molding process, this layer of shells ends up aligned at the edge of the molded structure, i.e., against the mold. Adding to this is the rms roughness of the EPS surface, typically several hundred micrometers. Projected at the incidence angles at which the specular reflectance was measured, the thickness of the outer shell layer with $n = 1.6$ is comparable to a wavelength or more. Thus the reflectance from the EPS surface at these incidence angles is higher, being weighted towards that of a material with $n = 1.6$ to a greater extent than if only examining the density-based effective refractive index of expanded polystyrene beads.

Table 2. Specular reflectances. For each EPS type measured, the incidence angle of the BWO beam is given, and the peak of the measured specular reflectance relative to the beam transmitted through the EPS.

		Density		
		35 g/L	54 g/L	120 g/L
Bead size	$d < 0.5 \text{ mm}$	n/a	n/a	$\theta_i = 52.5^\circ$ -23.5 dB
	$0.5 \text{ mm} < d < 0.7 \text{ mm}$	$\theta_i = 57.1^\circ$ -31.1 dB	$\theta_i = 57.5^\circ$ -26.2 dB	n/a

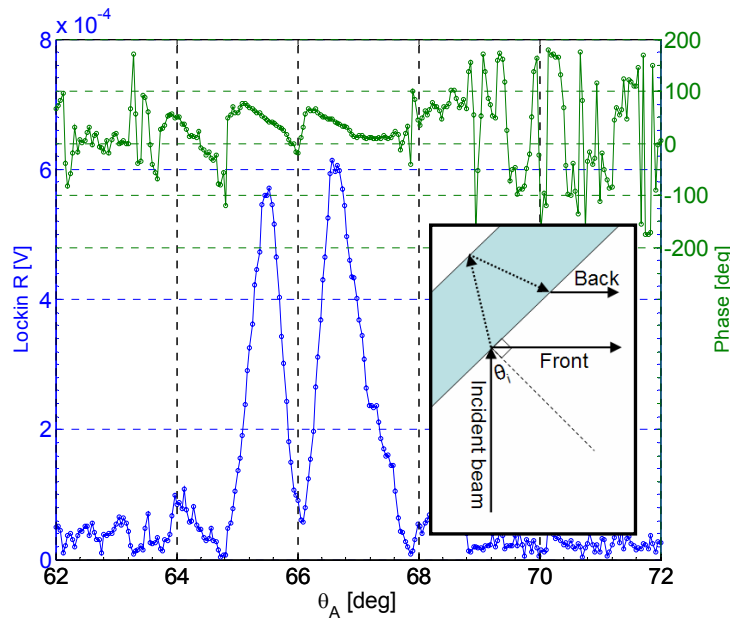


Fig. 4. Example of specular reflectance measurement, for $0.5 \text{ mm} < d < 0.7 \text{ mm}$, 54 g/L EPS, and $\theta_i = 57.5^\circ$. Arm angle θ_A is related to BWO beam incidence angle by $\theta_i = (180 - \theta_A)/2$. Reflection peaks are separated by 1° , corresponding to the reflections due to the front and back surfaces of the EPS thickness projected by the incidence angle (1.89 cm), viewed by a detector at the end of the periscope arm at θ_A . A schematic of the reflectance measurement geometry from an EPS sample is inset.

3.3 EPS forward scattering effects

An interesting result was observed for most EPS samples measured while acquiring data for Sections 3.1 and 3.2. In addition to the slight attenuation of the transmitted beam, coherent forward scattering was found. Essentially, it exhibited grating lobes with peaks typically greater than those of the specular reflections, at seemingly arbitrary locations. The locations of the lobes are based on the quasi-periodicity of the EPS, which is at some level a random medium, but is essentially comprised of a matrix of spheres expanded within a mold. In the ideal case of all spheres being identically sized, the spheres become rhombic dodecahedra – the most efficient use of space in the classic sphere-packing problem. Although neither the initial sphere diameters nor the final expanded bead sizes are uniform (the condition required for an analytic close-packing solution), it is clear that the EPS is periodic enough at certain positions and incidence angles to create grating lobes. Data from two EPS samples are shown in Figure 5. A 120 g/L, $d < 0.5$ mm sample at $\theta_i \sim 45^\circ$ is on the left; due to this particular EPS being relatively dense, this example demonstrates two effects simultaneously: extinction of the main beam and the forward-scattering grating lobes. Extinction of the main beam is due to scattering, absorption, and reflection of the incident beam out of the measurement region. The extinction relative to the no-sample beam is 5.6 dB. On the right is a 54 g/L, $0.5 \text{ mm} < d < 0.7 \text{ mm}$ sample at normal incidence. The scattering features are mostly symmetric.

Table 3 summarizes the percentages of scattered power found outside the main beam, in the plane of the measurement, for all EPS samples measured. Because the experimental setup does not allow two-dimensional measurements, we make the assumption that the incident beam is circular, as expected from the pattern given by a circular aperture, and also that the scattering features – grating lobes – are also circular. We note that the FWHMs of the scattering features are approximately the same as of the main beam, so percentages in Table 3 are calculated by subtracting the measured pattern with the sample out from the measured pattern with the sample in, and dividing the difference by the power summed in the main beam (denoted by the horizontal dashed line in Figure 5). The main beam is defined by the crossover point between the sample-in and sample-out power vs. angle measurements. In this situation, this crossover point is a more convenient definition of the “main beam” than the typical FWHM definition.

Table 3. EPS sample description, BWO beam incidence angle and percentage of power scattered relative to the BWO beam with no sample, and percentage of power scattered relative to the measured transmitted beam. The thick dashed horizontal line in Figure 5 represents the cutoff point for the “main beam”, both for the actual BWO pattern as well as the pattern measured with an EPS sample in place.

Sample	θ_i	Power scattered relative to original (no-sample) beam [%]	Power scattered relative to transmitted (sample) beam [%]
$d < 0.5$ mm, 35 g/L	0°	0.009	0.0015
$d < 0.5$ mm, 35 g/L	45°	0.009	0.0011
$d < 0.5$ mm, 120 g/L	0°	1.02	1.72
$d < 0.5$ mm, 120 g/L	45°	1.09	4.07
$0.5 \text{ mm} < d < 0.7 \text{ mm}$, 35 g/L	0°	0.035	0.035
$0.5 \text{ mm} < d < 0.7 \text{ mm}$, 35 g/L	45°	0.026	0.033
$0.5 \text{ mm} < d < 0.7 \text{ mm}$, 54 g/L	0°	0.98	1.21
$0.5 \text{ mm} < d < 0.7 \text{ mm}$, 54 g/L	45°	1.12	1.25

Though not shown graphically here, we found that nearly all forward scattered radiation lies within $\pm 15^\circ$ of the transmitted beam. As a common “transparent” structural material in the millimeter-wave/terahertz frequency range, this is of great use to know. Additionally, the magnitude of the scattered lobes is on the order of 1% for the most dense EPS, and reduces to 0.1% for the least dense samples. It is necessary to explicitly note that our measurements were performed in a single plane, and that generalization to the full hemisphere beyond the EPS plane requires an explanation. It is possible that in every measurement, either the sample or the periscope was slightly misaligned such that the axis of strong scattering (the plane of the incident beam) was not properly sampled. However, eight independent measurements of four samples were made without extensive care to ensure exact angular positioning of the sample, and because we can clearly see that scattered power is proportional to density, it is highly likely that the conclusions drawn from these 1D

measurements are extensible to the half space. Furthermore, the location and angular orientation of the EPS sample is no more accurate than the feature sizes of the sample itself, meaning that the orientation and position of the semi-infinite matrix of expanded polystyrene beads is essentially random, relative to the incident beam.

We have attempted to make a budget for radiation transmitted through EPS, separating the total incident power into reflected, transmitted, and scattered components. For reflected power, it is required to examine the inhomogeneity of the EPS to account for the refractive index being higher than expected due simply to density alone. The measurements of transmitted beam attenuation indicate greater attenuation than due to simply absorption and reflection from a slab of reduced-density polystyrene, but measurements of forward scattered power are able to account for the difference, excepting the densest sample.

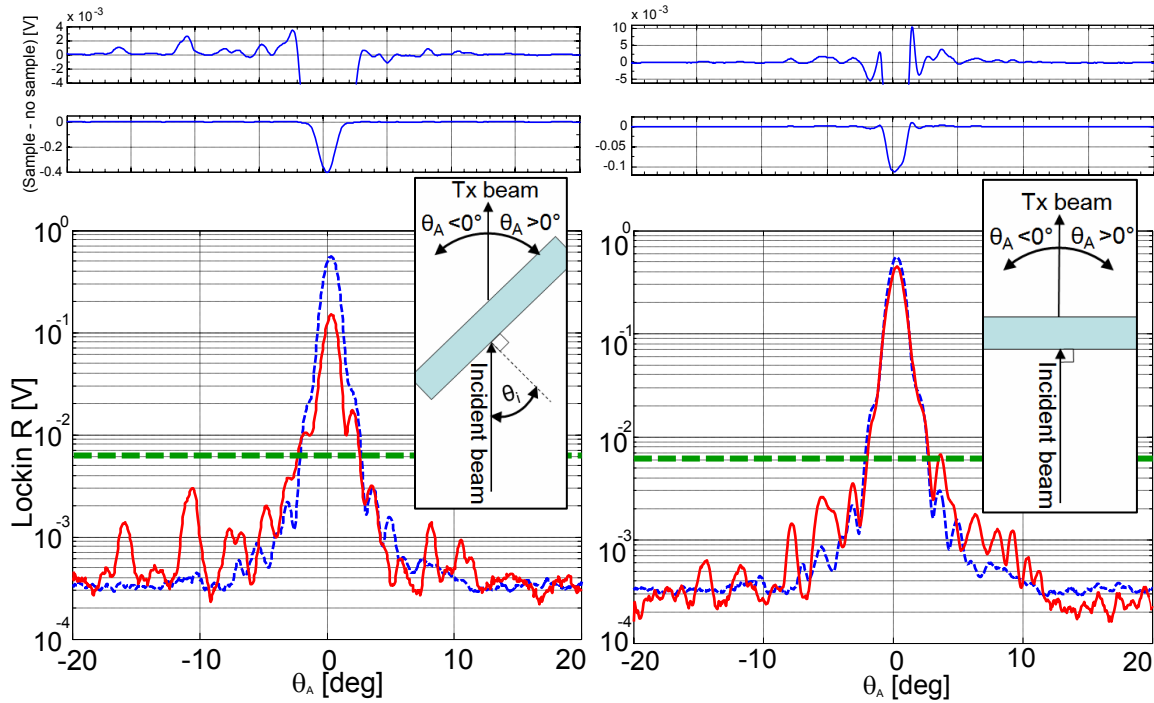


Fig. 5. (bottom left) Solid line: transmitted beam, through a $d < 0.5$ mm, 120 g/L EPS sample, at $\theta_i = 45^\circ$. Dashed line: beam with no sample (ensemble mean, same as Figure 3). The primary forward scattering features are seen at -16° and -10.5° . The main beam is attenuated due to a combination of reflection and true absorption. The thick dashed horizontal line indicates the “main beam” cutoff level, for purposes of calculating scattered radiation out of the main beam (Table 3). (top left) Difference between measurement of EPS (sample) and power-vs.-angle pattern with no EPS (no sample). Note that two linear scales are required to capture the dynamic range of the difference. (right) 0.5 mm $< d < 0.7$ mm, 54 g/L EPS sample measured at $\theta_i = 0^\circ$.

4. DISCUSSION

We have described a basic experimental setup for measurement of angular distribution of power in one plane. Measurement of coherent forward scattering – grating lobes – from EPS was observed for the first time, and the scattered power in the plane of the measurement was found to be between 0.01% and 1.1% dependent on EPS density. We found that nearly all forward scattered radiation lies within $\pm 15^\circ$ of the transmitted beam. As a common “transparent” structural material in the millimeter-wave/terahertz frequency range, this is of great practical knowledge. Refractive index was determined by measurement of specular reflectance and found to agree with other work in the 35 g/L EPS sample ($n = 1.035$), but was calculated to be $n = 1.14$ - 1.15 for the highest density EPS sample, rather than the 1.06 or 1.07 predicted by polystyrene density alone. This is attributed to the non-uniform density profile of the expanded polystyrene beads, affecting the apparent refractive index at incidence angles close to glancing.

C.R. Dietlein is funded by National Science Foundation grant #0501578: interdisciplinary research in submillimeter-wave imaging.

REFERENCES

- [1] J.E. Bjarnason, T.L.J. Chan, A.W.M. Lee, M.A. Celis, and E.R. Brown, "Millimeter-wave, terahertz, and mid-infrared transmission through common clothing," *Applied Physics Letters* 85 (2004): 519-521.
- [2] N.A. Salmon, R. Appleby, and S. Price, "Scene simulation of passive millimeter-wave images of plastic and metal objects," R. Appleby, G.C. Holst, and D.A. Wikner, Eds., vol. 4719, no. 1. SPIE, 2002, pp. 397-401.
- [3] N.A. Salmon, "Polarimetric scene simulation in millimeter-wave radiometric imaging," R. Trebits, J.L. Kurtz, R. Appleby, N.A. Salmon, and D.A. Wikner, Eds., vol. 5410, no. 1, SPIE, 2004, pp. 260-269.
- [4] R. Appleby and M.L. Musselwhite, "Millimeter-wave reflectometer," R. Appleby, G.C. Holst, and D.A. Wikner, Eds., vol. 4719, no. 1. SPIE, 2002, pp. 402-408.
- [5] C.R. Dietlein, Z. Popovic, and E.N. Grossman, "Broadband THz aqueous blackbody calibration source," R. Appleby and D.A. Wikner, Eds., vol. 6548, no. 1, SPIE, 2007.
- [6] G. Zhao, M. Mors, T. Wenckebach, and P.C. Planken, "Terahertz dielectric properties of polystyrene foam," *J. Opt. Soc. Am. B*, pp. 1476-1479, June 2002.
- [7] A. Luukanen, E.N. Grossman, A.J. Miller, P. Helistö, J.S. Penttilä, H. Sipola, and H. Seppä, "An Ultra-Low Noise Superconducting Antenna-Coupled Microbolometer With a Room-Temperature Read-Out," *IEEE Microwave and Wireless Components Letters*, pp. 464-466, 2006.
- [8] Penttilä, J.S., H. Sipola, P. Helistö, and H. Seppä, "Low-noise readout of superconducting bolometers based on electrothermal feedback," *Superconductor Science Technology* 19, pp. 319-322, April 2006.
- [9] A.T. Lee, P.L. Richards, S.W. Nam, B. Cabrera, and K.D. Irwin, "A superconducting bolometer with strong electrothermal feedback," *Applied Physics Letters* 69, pp. 1801-1803, 1996.
- [10] C.R. Dietlein, J.D. Chisum, M. Ramirez, E.N. Grossman, A. Luukanen, Z. Popović, "Integrated microbolometer antenna characterization from 95-650 GHz," [IEEE MTT-S IMS Digest](#), 1165-1168, 2007.
- [11] D. Rogers, Tempo Plastic Company (private communication).
- [12] R. Piesiewicz, C. Jansen, S. Wietzke, D. Mittleman, M. Koch, and T. Kurner, "Properties of building and plastic materials in the THz range," *International Journal of Infrared and Millimeter Waves*, vol. 28, no. 5, pp. 363-371, May 2007.
- [13] C.F. Bohren and D.R. Huffman, *Absorption and scattering of light by small particles*, pp. 30-41 Wiley-VCH, 1998.
- [14] M. Plonus, "Theoretical investigations of scattering from plastic foams," *IEEE Trans. Antennas and Propagation*, vol. 13, no. 1, pp. 88-94, 1965.